JOURNAL OF GEOPHYSICAL RESEARCH, VOL. 112, A10313, doi:10.1029/2007JA012366, 2007

Reversed flow events in the winter cusp ionosphere observed by the European Incoherent Scatter (EISCAT) Svalbard radar

Y. Rinne,[1] J. Moen,[1,2] K. Oksavik,[3] and H. C. Carlson[1,4]

Received 27 February 2007; revised 13 June 2007; accepted 20 June 2007; published 31 October 2007.

[1] High-resolution fast azimuth sweeps by the European Incoherent Scatter (EISCAT) Svalbard radar provide an unparalleled opportunity to study small-scale flow disturbances in the cusp ionosphere. Observations from 11 days of the winter cusp ionosphere of high-resolution ion flow data have been analyzed. Transient channels of reversed plasma flow appear to be a regular feature of the cusp, and they were seen in 16% of 767 analyzed EISCAT Svalbard Radar (ESR) scans. We introduce a new descriptive term, reversed flow events (RFEs), for this class of events. RFEs are defined as longitudinally elongated segments of transiently enhanced ion flow in the direction opposite to the background flow. RFEs typically occurred near the cusp inflow region in association with enhancements in the polar cap convection observed by the Super Dual Auroral Radar Network (SuperDARN). Their lifetime was found to be ~19 min on average. Their longitudinal dimension typically exceeded the ESR field of view (>400–600 km), and ranged from ~50 to 250 km in latitude. The occurrence rate of RFEs appears independent of the B_Z and B_Y component polarity of the interplanetary magnetic field (IMF), and RFEs occurred for clock angles between 40° and 240°. RFE ion flow was in 95% of the cases documented to oppose the magnetic tension force, and RFEs cannot be interpreted in terms of newly opened flux. RFEs formed one by one and never simultaneously in pairs. To explain these observations, we propose an asymmetric version of the Southwood (1987) twin cell flux transfer event model to account for significant IMF B_Y, in which only the poleward cell located on open field lines develops.

Citation: Rinne, Y., J. Moen, K. Oksavik, and H. C. Carlson (2007), Reversed flow events in the winter cusp ionosphere observed by the European Incoherent Scatter (EISCAT) Svalbard radar, *J. Geophys. Res.*, *112*, A10313, doi:10.1029/2007JA012366.

1. Introduction

[2] Magnetic reconnection was first described by *Dungey* [1961] as a steady process. Several years later, *Russel and Elphic* [1978, 1979] and *Haerendel et al.* [1978] found evidence for a pulsed nature of the reconnection process. This transient, impulsive reconnection at the dayside magnetopause is called flux transfer events (FTEs). The first radar observations of FTE flow transients were carried out by *van Eyken et al.* [1984] and *Goertz et al.* [1985].

[3] *Southwood* [1987] proposed a model of the plasma flow associated with the ionospheric footprint of an FTE, hereafter referred to as the Southwood model. According to this model, a pair of field-aligned currents (FAC) with opposite polarity flows on the poleward and equatorward edge of the newly reconnected flux tube and transfers stress to the ionosphere. The resulting motion of the foot of the flux tube through the ionosphere sets up a twin vortex flow pattern. This pattern is understood as the newly opened flux moving faster than the surrounding flux, pushing its way through the plasma and thereby creating return flow on either side.

[4] Over the past 2 decades there have been made many attempts to find observational evidence for the Southwood model. *Lockwood et al.* [1989] and *Sandholt et al.* [1990] suggested that discrete cusp auroral events are related to flow shears consistent with the clockwise cell of the Southwood FTE model. However, *Lockwood et al.* [1990] suggested that the return flow in the Southwood model may not be very pronounced, but rather a reduction in the background convection. *Denig et al.* [1993] reported evidence for a Southwood FTE twin-cell moving with the large-scale convection. *Pinnock et al.* [1993] reported the observation of a "longitudinally elongated (>900 km), latitudinally narrow (~100 km) channel of enhanced convection" by combining observations from the PACE high-frequency (HF) radar and the DMSP F9 polar-orbiting satellite. Within the channel, the line-of-sight velocity of the plasma was enhanced compared to the background flow. In the regions bordering the channel, the background flow was diminished, however not reversed. *Pinnock et al.* [1993] interpreted the weakening of the background convection as return flow in the Southwood model as proposed by *Lockwood et al.* [1990].

[1]Department of Physics, University of Oslo, Oslo, Norway.
[2]Arctic Geophysics, University Centre in Svalbard, Longyearbyen, Norway.
[3]Johns Hopkins University Applied Physics Laboratory, Laurel, Maryland, USA.
[4]Center for Atmospheric and Space Sciences, Utah State University, Logan, Utah, USA.

0148-0227/07/2007JA012366$09.00

[5] *Marchaudon et al.* [2004] observed an azimuthally elongated convection enhancement by two Super Dual Auroral Radar Network (SuperDARN) radars in conjunction with FACs observed by the Ørsted satellite. They found that the direction of the FAC pair was in entirely agreement with the Southwood model. Furthermore, the current densities of each FAC and the Pedersen current indicated that the closure current for the pair of FACs was inside the flow burst. The dimensions of the ionospheric convection enhancement were 1000 km in length and 100 km in width, and the flow was larger than 1000 m/s, exceeding the background flow. *Marchaudon et al.* [2004] claimed the validity of the Southwood model based on their observations.

[6] The development of the Special Norwegian Fast Azimuth Scan Mode (SP-NO-FASM) for the European Incoherent Scatter (EISCAT) Svalbard Radar (ESR) by *Carlson et al.* [2002] provided a new tool to map out flow patterns with high spatial and temporal resolution. *Oksavik et al.* [2004, 2005] reported the first high resolution measurements of the flow disturbance around poleward moving auroral forms (PMAFs) by this radar technique. *Oksavik et al.* [2004] concluded that the spatial structure of a small-scale twin-cell system was in accordance with the Southwood prediction. The enhanced convection channel interpreted as the center flux in the Southwood model was only 50–60 km wide, and surrounded by flow running in the opposite direction. The PMAF was situated at the poleward edge of the flow channel thereby being consistent with the signature of an upward Birkeland current filament as predicted by the Southwood model. *Oksavik et al.* [2005] presented a train of narrow flow channels associated with a sequence of PMAFs. They plausibly related reversed flow channels to flux transfer events.

[7] *Neudegg et al.* [2000] showed that reconnection bursts at the magnetopause may take place for a wide range of clock angles from 30° to 330°. Hence if reversed flow channels represent an observable FTE signature, such as stated by *Oksavik et al.* [2005], they should be a frequently occurring phenomenon in the SP-NO-FASM database. In this study, the available SP-NO-FASM database has been analyzed systematically with the aim to characterize the occurrence and lifetime as well as dependency on magnetic local time (MLT) and interplanetary magnetic field (IMF) conditions of transient flow channels with reversed plasma flow with respect to the background convection. We focus on the RFE events as they have not been resolved by other radars and hence represent a new observable feature. Interestingly, we find that RFE events never develop in pairs, which means that they cannot be a symmetric Southwood FTE pattern.

[8] This paper is structured in the following way: Section 2 describes the instrument modes and techniques used in the study; section 3 introduces the data set and the analysis criteria that were used by providing one event as an example. Section 4 presents the results, followed by the discussion in section 5 and a summary in section 6.

2. Instrument Modes and Techniques

[9] This section provides brief descriptions of the ESR scan mode that has been used to gather the data (section 2.1), the SuperDARN global convection maps (section 2.2), and how the time lag between the Advanced Composition Explorer (ACE) satellite and the ionospheric response has been calculated (section 2.3).

2.1. ESR Scan Mode

[10] The primary data source in this paper is ionospheric line-of-sight data from the SP-NO-FASM program at the ESR which is located in Longyearbyen (78.15°N and 16.03°E). This windshield wiper mode was originally designed by *Carlson et al.* [2002] to monitor the formation of polar cap patches near the cusp inflow region with an unprecedented combination of wide area coverage (~600 km in width × 1000 km in length), quick scan time (2 min), and fine spatial resolution (~15 km × 30 km). Magnetic noon at the ESR site corresponds to 0900 universal time (UT).

[11] In the SP-NO-FASM program, the ESR 32 m steerable antenna sweeps azimuthally back and forth at a fixed elevation angle of 30°. The sweeps follow the surface of a cone. The azimuth angle is determined with respect to geographic north (0° and 360°) increasing clockwise. The elevation angle is the angle with the horizon increasing from 0° to 90° at zenith. In the discussion to follow elevation refers to the angle between the radar dish pointing direction and the local horizon; i.e., so that 150° elevation and 0° azimuth will be referred to as 30° elevation and 180° azimuth. The transmission pulse code used for the SP-NO-FASM program is tau0, consisting of two 960 μs alternating codes that are sampled every 16 μs (2.4 km). The first of the two alternating codes, AC1, covers ranges from 212 to 1306 km, whereas the second, AC2, covers the region between 58 and 1153 km. Data is stored every 3.2 s, and each 3.2 s data set has been analyzed separately.

[12] Reconnection signatures can be expected in the dayside boundary layers, the low-latitude boundary layer (LLBL), cusp, and mantle. These boundary layers typically span from 0900 to 1500 MLT [*Newell and Meng*, 1992] but due to IMF B_Y controlled shifts around magnetic noon may start as early as 0600 MLT and end as late as 1800 MLT [*Milan et al.*, 2000; *Moen et al.*, 2001; *Newell et al.*, 2004]. The width of the instantaneous active cusp may be at least 4 hours or more in MLT [*Maynard et al.*, 1997]. Under moderate conditions the daytime auroral precipitation region is located around 75° magnetic latitude (MLAT), but depending on IMF B_Z strength and polarity the precipitation region and reconnection signatures may be located between 70° and 80° MLAT [*Sandholt et al.*, 1998].

[13] In this radar study we have not made any attempt to locate the cusp precipitation region. However, during the campaign the ESR sweeps were directed toward where the active cusp region was assumed to be for the prevailing IMF conditions and MLT. Scanning at a constant elevation of 30° the radar field of view extends over ~1.5 hours in MLT along the line-of-sight if pointed directly east or west, and ~7° in latitude if pointed north or south. The fan-shaped field of view spanned usually 90–120° in azimuth throughout the data set, which means that the ESR can give an instantaneous snapshot of up to half the area of the cusp at one time. If the ESR was situated in the middle of the cusp and was scanning 360° in azimuth, it could in principle see most of the cusp except from a large "doughnut hole"

Table 1. Overview of Available European Incoherent Scatter (EISCAT) Svalbard Radar (ESR) Data and Specification of the Scan Modes Used

Date (2001)	Available ESR Data	Elevation, deg	Azimuth, deg	Azimuth Width, deg	Period, s	Speed, deg/s	Excluded Scans	Number of Scans	Center MLT
16.01.	06:03:10–07:38:34	30	−75 to 15	90	128	0.703	None	45	08:33:10–10:08:34
16.01.	08:34:22–11:01:34	30	−165 to −75	90	128	0.703	9:10, 9:20, 11:01	64	10:24:22–12:51:34
17.01.	06:01:02–07:15:07	30	15 to 105	90	128	0.703	6:01, 6:11, 6:13	32	10:11:02–11:25:07
17.01.	09:16:02–10:50:38	30	−75 to 15	90	128	0.703	9:16,	44	11:46:02–13:20:38
18.01.	06:05:07–07:34:18	30	30 to 90	60	192	0.313	All	0	09:05:07–10:34:18
19.01.	06:02:38–07:57:47	30	15 to 105	90	128	0.703	None	54	10:12:38–12:07:47
19.01.	09:31:42–11:59:46	30	−75 to 15	90	128	0.703	11:58	69	12:01:42–14:29:46
20.01.	06:03:02–07:17:17	30	15 to 105	90	128	0.703	6:19–6:34 (7 scans)	28	10:13:02–11:27:17
20.01.	09:55:22–10:59:54	30	−75 to 15	90	128	0.703	10:59	30	12:25:22–13:29:54
15.12.	06:03:54–07:46:15	30	0 to 120	120	192	0.625	6:38, 7:01	26	10:13:54–11:56:15
15.12.	09:08:17–09:27:26	30	0 to 120	120	192	0.625	None	6	13:18:17–13:37:26
15.12.	09:28:30–10:59:54	150 (30)	0 to 120 (180–300)	120	192	0.625	None	29	11:18:30–12:49:54
16.12.	06:05:01–06:30:05	30	−60 to 60	120	192	0.625	None	8	07:55:01–08:20:05
16.12.	06:30:43–08:19:28	30	0 to 120	120	192	0.625	None	34	10:40:43–12:29:28
16.12.	08:20:06–09:30:24	30	−60 to 60	120	192	0.625	None	22	11:20:06–12:30:24
16.12.	09:31:28–10:59:54	150 (30)	0 to 120 (180–300)	120	192	0.625	None	28	11:21:28–12:49:54
17.12.	06:05:30–06:58:27	30	0 to 120	120	192	0.625	6:30, 6:52, 6:56	9	10:15:30–11:08:27
17.12.	10:01:01–10:59:44	150 (30)	0 to 120 (180–300)	120	192	0.625	10:58	19	11:51:01–12:49:44
18.12.	06:31:02–08:06:59	30	0 to 120	120	192	0.625	8:03	29	10:41:02–12:16:59
18.12.	09:22:59–10:31:47	150 (30)	0 to 120 (180–300)	120	192	0.625	10:30	21	11:12:59–12:21:47
18.12.	10:45:10–10:59:54	30	−225 to 135	360	512	0.703	None	2	13:45:10–13:59:54
19.12.	06:00:51–08:20:26	30	0 to 120	120	192	0.625	8.08, 8:17	41	10:10:51–12:30:26
19.12.	08:22:11–08:47:38	150 (30)	0 to 120 (180–300)	120	192	0.625	None	8	10:12:11–10:37:38
20.12.	06:00:01–07:58:22	30	0 to 120	120	192	0.625	7:37	33	10:10:01–12:08:22
20.12.	10:06:47–10:57:56	150 (30)	0 to 120 (180–300)	120	192	0.625	None	16	11:56:47–12:47:56
21.12.	06:00:38–10:59:15	30	−180 to 180	360	256	1.406	None	70	09:00:38–13:59:15

around Longyearbyen, resulting from the fact that the SP-NO-FASM does not receive data from below 200 km altitude or overhead the radar site.

2.2. SuperDARN Global Convection Maps

[14] SuperDARN consists of a network of HF radars with overlapping fields of view in the northern and southern hemispheres. HF radars are sensitive to backscatter from field-aligned ionospheric irregularities in the order of decameters. The main purpose of SuperDARN is to provide global and continuous observations of the large-scale ionospheric convection pattern. These convection maps are produced by combining the line-of-sight velocity data from the entire SuperDARN network in one hemisphere and information from a statistical model parameterized by IMF conditions where no velocity measurement is available. The technique was first developed by *Ruohoniemi and Baker* [1998] and has later been refined by *Shepherd and Ruohoniemi* [2000].

[15] In order to put the plasma convection and mesoscale features monitored by the ESR into a global polar cap convection context, SuperDARN convection maps were used. These convection maps were retrieved from the Johns Hopkins University Applied Physics Laboratory (JHU/APL) Web site and are averaged over 2 min. A new map is available every 10 min.

2.3. ACE IMF Data

[16] In order to put an event in the ionosphere in the context of IMF, it is necessary to determine the time lag between the ACE satellite orbiting the first Lagrange point and the ionospheric response.

[17] This propagation delay from ACE to the magnetopause was estimated by averaging the solar wind bulk speed and the geocentric solar magnetospheric (GSM) X coordinate for the satellite position over a time period of 1 hour around an event (30 min before and after event onset/stop). The position of the magnetopause was calculated by the formula used by *Rodger* [1998] and a 6 min delay was added to the total time lag to account for the propagation time from the magnetopause to the *F* region ionosphere [*Moen et al.*, 2004].

3. Presentation of the Database and Analysis

[18] This section starts by presenting the database (section 3.1), followed by a description of the criteria that have been used to analyze the data (section 3.2), and it concludes by giving an example of an RFE (section 3.3).

3.1. Database

[19] The data set examined in this study consists of all ESR line-of-sight data from daytime SP-NO-FASM scans at constant 30° elevation during 12 days between 16–20 January 2001 and 15–21 December 2001. All data have been checked carefully for quality, and intervals of transmitter problems affecting the reliability of the ion velocity measurements have been removed. This was the case for three scans from 17 January 2001 (0601–0602, 0611–0613, and 0613–0615 UT), seven scans from 20 January 2001 (0619–0634 UT), and all data on 18 January 2001. Furthermore, 18 incomplete scans were also excluded. The remaining data set consists of 35 hours and 49 min of observations in a total of 767 scans. Table 1 lists the dates (first column) and time intervals (second column) of avail-

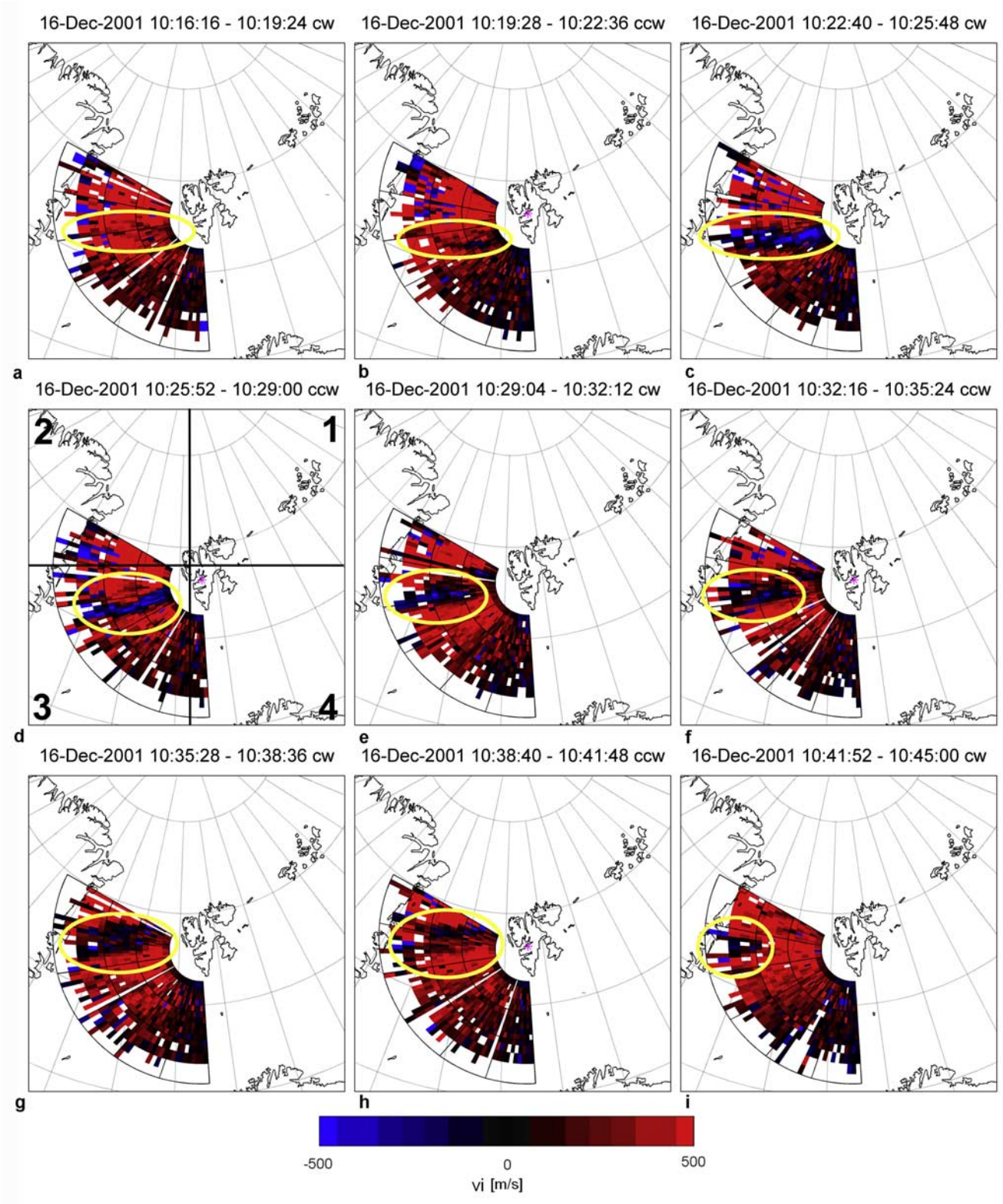

Figure 1. (a–i) A sequence of ion velocity fan plots from the European Incoherent Scatter (EISCAT) Fast Azimuth Scan Mode (FASM), in geographic coordinates. Data were projected along the magnetic field to a common reference altitude of 250 km. Positive velocities indicates line-of-sight ion flow directed away from the radar. The date and time as well as the radar sweep direction (clockwise "cw" and counterclockwise "ccw") are indicated on the top of each figure. The reversed flow event (RFE) is marked by a yellow ellipse. The quadrant definition in Figure 1d is used to sort the occurrence of RFEs in geographic regions relative to the EISCAT Svalbard radar (ESR) site. According to the definition, the RFE, seen as a blue stripe inside the yellow ellipse, is located in the third quadrant.

able data. Details about the scan pattern are specified in columns 3–7. Columns 3–5 list the constant elevation angle, the azimuth range and the azimuth width covered by a single sweep, and columns 6 and 7 contain the time it takes to complete a single sweep and the azimuthal speed of the ESR dish. The scans that are not used in the analysis are listed in column 8, and column 9 specifies the total number of scans that went into the analysis for each time period.

[20] Depending on the azimuth range, the ESR field of view extends 2–4 hours in MLT. The MLT listed in column 10 refers to the centre position in longitude of the ESR field of view.

[21] Since the ESR scans are at 30° elevation, the data is obtained from increasing altitude for increasing distance from the ESR site. In order to ease the comparison with data from other sources there is a need to project the data to a common reference altitude. At altitudes where collisions between charged particles and neutrals can be ignored, the frozen-in concept is valid and both electron and ions drift with same velocity perpendicular to the electric field. This is typically the case in the *F* region ionosphere above 200 km. As shown in Figure 1 (ion velocity plot), we have therefore projected the primary plasma parameter v_i along the magnetic field to a common reference altitude of 250 km, an altitude conventionally assumed for 630.0 nm optical emissions. Positive ion velocities (red) are directed away from the radar along the line of sight, whereas negative velocities toward the radar along the line of sight are colored blue. Missing data values are plotted as white.

3.2. Analysis Criteria

[22] Since the ion drift velocity data contained much fine structure, clear and strict selection criteria had to be defined:

3.2.1. Reversed Flow Event (RFE) Definition

[23] An RFE, or flow channel, is an elongated segment of enhanced ion flow in the opposite direction to the background flow. The background flow is the large-scale plasma convection in the polar cap. SuperDARN convection maps were retrieved from JHU/APL and used to verify the large-scale flow context of the ESR observations. In order for an event to qualify as RFE the following criteria have to be fulfilled:

[24] 1. The RFE has to be evident in more than one radar beam direction (azimuth position). This criterion eliminates questionable measurements.

[25] 2. The line-of-sight ion drift velocity inside the RFE must be >|250| m/s for at least one scan during the lifetime of the event.

[26] 3. The longitudinal extent of an RFE has to exceed 400 km in the radar field of view.

[27] 4. The RFE has to stay in clear contrast to the background flow, i.e., the background flow must exhibit uniform and opposite velocities >|250| m/s in the area surrounding the RFE for at least one scan.

[28] 5. The RFE has to be embedded within the background flow for at least one scan (this criterion avoids large-scale convection reversals being detected as RFE).

3.2.2. Flow Structure Definition

[29] Flow signatures which do not satisfy all criteria but resemble the beginning of an RFE (like in Figures 1a and 1b (1016 and 1019 UT)) have been classified as "flow structures."

[30] In addition to the fact that the ESR field of view is only capable of seeing parts of the active cusp and that there are uncertainties with regard to the exact location of the cusp, the direction of plasma flow inside an RFE as well as the orientation of the background convection is important for whether or not the ESR is sensitive to flow events. The ESR is only sensitive to plasma motion along its line-of sight, and insensitive to plasma flow perpendicular to the pointing direction. According to point 4 of the RFE definition, the background flow must exhibit uniform velocity higher than ±|250| m/s along the line-of-sight in the region of the RFE and the RFE itself must be higher than ±|250| m/s in the opposite direction. Hence RFEs cannot be detected when either the large-scale background convection and/or the RFE flow channel is oriented perpendicular to the radar line of sight. Assuming an ion flow velocity of ~1000 m/s, the ±|250| m/s criterion means a maximum angle between the flow vector and ESR line of sight of 75°. Any larger offset will result in an ion flow component along the ESR line of sight less than |250| m/s and hence not qualify for RFE detection.

3.3. An Example RFE

[31] Figure 1 shows a typical example of an ESR scan sequence. The nine scans on the 16 December 2001 from 1016 UT to 1045 UT indicate the development of an RFE in the ESR field of view. The RFE is highlighted by a yellow ellipse in each figure. As can be read from Table 1 column 4, the ESR scanned 120° azimuth from 180° to 300°. The background plasma convection monitored by the ESR is uniform and predominantly directed westward except from the southern part of the scan where the ESR line of sight velocity is not sensitive to zonal flow.

[32] Before we consider the high-resolution flow data in more detail, we will present the large-scale context provided by SuperDARN. Figure 2 shows a sequence of SuperDARN convection maps covering the whole time period of the RFE, with the ESR field of view indicated. SuperDARN had good coverage in the ESR field of view. Svalbard was located slightly postnoon in a region of high plasma convection directed mostly northwestward. This convection pattern is consistent with the background flow seen by the ESR.

[33] The IMF conditions for this time period are shown in Figure 3. As can be seen, IMF B_Y was strongly positive during the whole time interval. IMF B_Z was positive as well, except for a brief negative excursion around 1035 UT. The SuperDARN polar cap convection pattern exhibited a twin cell nature, indicative of reconnection driven flows, and the well-developed dusk convection cell is consistent with positive IMF B_Y.

[34] Having in mind that the ESR field of view was situated under westward large-scale convection in the postnoon sector, we return to Figure 1. The RFE started out as a reduction of the background flow (1016–1019 UT) before it rapidly developed to a pronounced channel of strongly reversed ion flow with respect to the background convection (seen from 1022–1025 UT). From 1029 to 1045 UT, the RFE moved northward and weakened before fading. Such narrow, well-defined, transient small-scale flow channels have been found frequently throughout the data set. Some, but not all, broaden and/or move north/south before they

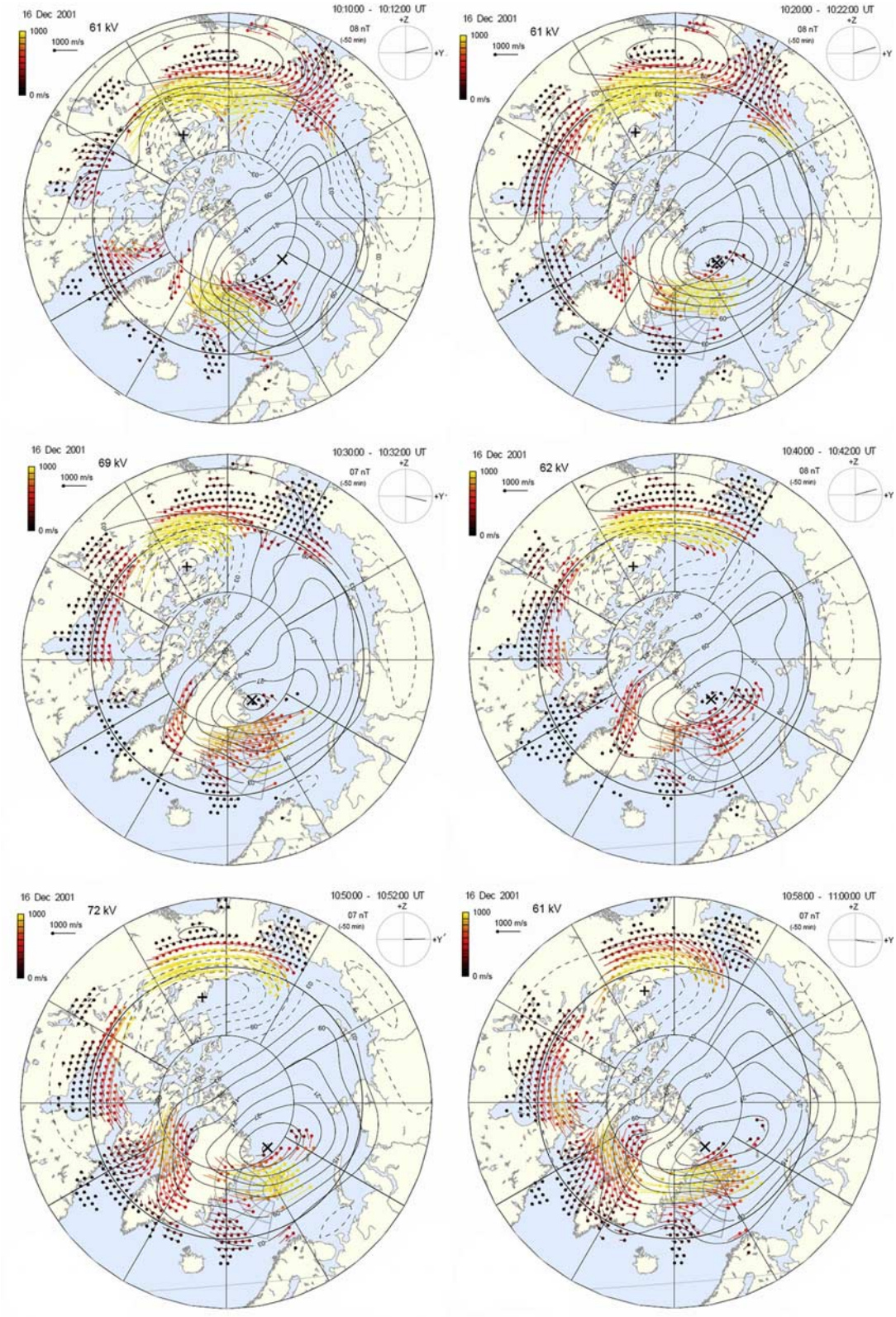

Figure 2. A sequence of SuperDARN global convection patterns, in magnetic coordinates. Indicated are polar cap potential contours and flow vectors based on SuperDARN measurements of the convection. Noon (1200 MLT) is at the bottom of each figure. In addition, the ESR field of view has been superimposed. The global convection maps were retrieved from the Johns Hopkins University Applied Physics Laboratory (JHU/APL). They are averaged over 2 min and a new map is available every 2 min. A propagation time from ACE to the ionospheric response of 50 min was assumed, which is consistent with the 47 min calculated for the actual time period (see section 2.3).

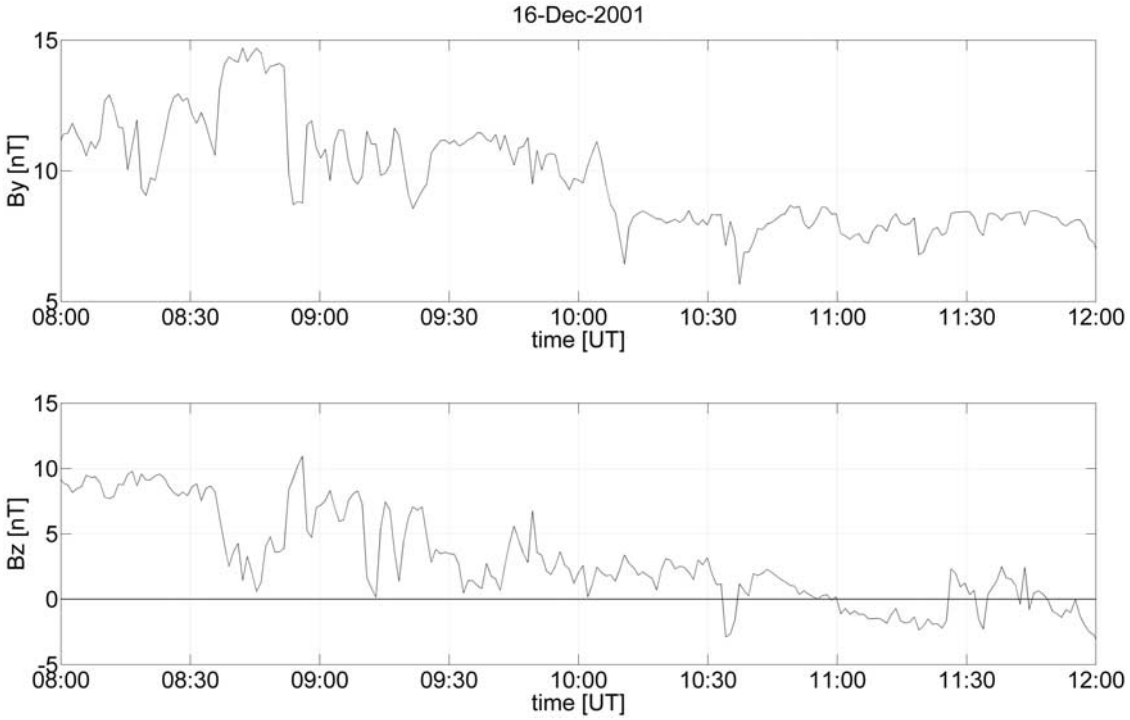

Figure 3. ACE measurements of the IMF B_Y and B_Z components between 0800 and 1200 UT on 16 December 2001. The time axis accounts for a time delay of 47 min from the spacecraft to the ionosphere. The time axis shown is thus time_{ACE} + 47 min.

fade. A number of flow structures have been found where a region of the background convection has reversed or diminished, as in Figures 1a and 1b from 1016–1022 UT. Unlike the case presented in Figure 1, however, these flow structures did not develop into RFEs.

4. Results

[35] This result section is divided into two main parts. The first part (section 4.1) explains the columns in Table 2 which lists the RFEs and flow structures identified in the dataset together with some attributes for further analysis. The second part (section 4.2) states the results of the analysis and is divided into three subsections (4.2.1–4.2.3) that elaborate on different aspects of the RFE occurrence.

4.1. Explanation of the Columns in Table 2

[36] Number indicates the serial number of a given RFE or flow structure. RFEs and Flow Structures are numbered separately. Class describes whether a given signature meets the criteria of a RFE (marked RFE) or a flow structure (marked FS). RFEs and their attributes are written in bold and flow structures in italic for easier distinction. Date lists the date when a given event or structure occurred. Start/End lists the start/stop times in UT of the first/last scan when an event was visible. The very first and last signs which could be associated with an RFE or flow structure have been taken as beginning and end times. Number of scans states the number of consecutive scans a given signature was visible. Dur. [s] (duration) gives the lifetime of one single RFE/flow structure. Q (quadrant) indicates in which of the four azimuthal quadrants of the ESR field of view an RFE or flow structure was located, as defined in Figure 1d. The particular RFE shown in Figure 1d, visible as a blue stripe inside the yellow ellipse, was located in the third quadrant. abs(v_i) is the absolute value of the ion velocity of the RFE or flow structure along the ESR line of sight, given within ranges of 0–250, >250 m/s. M (motion) indicates whether or not the RFE or flow signature moved north (N) poleward or south (S) equatorward. W (widening) indicates whether the RFE or flow signature widened throughout its lifetime, indicated by an "X." FOV (field of view) has an "X" set in this column whenever an event was cut short or its onset could not be observed as the radar field of view was altered to look in a different azimuth sector. "PD" (poor data) indicates that an RFE or structure was followed by questionable data. IMF B_Z states the polarity of IMF B_Z averaged over the lifetime of an event (cf section 2.3). The notation used is a plus symbol and a minus symbol for values larger or smaller than zero. IMF B_Y has the same notation as for IMF B_Z. θ (°) (clock angle) states the clock angle for RFEs and flow structures calculated from average IMF B_Y and B_Z values (see above). The clock angle is defined with respect to IMF B_Z north, increasing clockwise from 0 to 360° in the IMF B_Y/B_Z plane. SD Cov (SuperDARN coverage) indicates whether SuperDARN had data coverage at the location of the ESR field of view at any time. "N" means that there are no SuperDARN flow vectors at the location of the ESR fan, and convection is derived entirely based on the SuperDARN model [*Ruohoniemi and Baker*, 1998]. SD Match indicates if the large-scale convection observed by SuperDARN agreed with the line-of-sight measurements of the ESR, as determined qualitatively by eye inspection. F_t indicates whether or not the flow of an RFE was directed

Table 2. Occurrence of All Reversed Flow Events and Flow Structures Which Have Been Identified Throughout the Data Set With Columns Explained in Detail in Section 4.1

Number	Class	Date	Start	End	Number of Scans	Dur., s	Q	abs(v_i)	M	W	FOV	IMF B_Z	IMF B_Y	θ, deg	SD Cov	SD Match	F_t
1	FS	16.01.2001	0855	0859	2	256	3	> 250				–	+	154	Y	Y	
2	FS	16.01.2001	0859	0903	2	256	3	> 250				–	+	162	Y	Y	
3	FS	16.01.2001	0908	0910	1	128	3	> 250			PD	–	+	161	Y	Y	
4	FS	16.01.2001	0931	0933	1	128	3	0–250				–	–	212	Y	Poor	
1	**RFE**	**16.01.2001**	**1007**	**1016**	**4**	**512**	**3**	**> 250**				–	–	**237**	**Y**	**N**	**A**
5	FS	16.01.2001	1029	1033	2	256	3	> 250				–	+	174	Y	Y	
6	FS	16.01.2001	1050	1052	1	128	3	> 250				–	–	191	Y	Y	
7	FS	17.01.2001	0933	0935	1	128	2	> 250				+	+	39	N		
8	FS	19.01.2001	0611	0628	8	1024	1	> 250				+	+	44	Y	Y	
9	FS	19.01.2001	1027	1029	1	128	2	0–250				+	+	78	Y	Y	
10	FS	19.01.2001	1031	1033	1	128	2	0–250				+	+	71	Y	Y	
11	FS	19.01.2001	1035	1039	2	256	2	0–250				+	+	87	Y	Y	
12	FS	19.01.2001	1118	1122	2	256	2	0–250				–	+	152	Y	Y	
13	FS	19.01.2001	1135	1141	3	384	2	> 250				–	+	173	Y	Y	
14	FS	19.01.2001	1143	1146	1	128	2	> 250				–	+	175	Y	Y	
15	FS	19.01.2001	1154	1156	1	128	2	0–250				–	+	180	Y	Y	
2	**RFE**	**20.01.2001**	**0645**	**0649**	**2**	**256**	**1**	**> 250**	**N**			–	–	**189**	**Y**	**Y**	**O**
16	FS	20.01.2001	1001	1005	2	256	2	> 250				+	+	89	N		
17	FS	20.01.2001	1022	1027	2	256	2	> 250				+	+	73	N		
18	FS	20.01.2001	1022	1027	2	256	2	0–250	S			+	+	73	N		
19	FS	20.01.2001	1029	1031	1	128	2	0–250				+	+	67	N		
20	FS	20.01.2001	1031	1037	3	384	2	0–250				+	+	61	N		
21	FS	20.01.2001	1044	1048	2	256	2	0–250				+	+	53	N		
3	**RFE**	**15.12.2001**	**0736**	**0743**	**2**	**384**	**1**	**> 250**		**X**		–	**+**	**97**	**Poor**	**Y**	**O**
22	FS	15.12.2001	0914	0921	2	384	4	> 250				–	+	97	Y	Y	
4	**RFE**	**15.12.2001**	**0924**	**0927**	**1**	**192**	**1**	**> 250**				–	**+**	**90**	**Y**	**Y**	**O**
23	FS	15.12.2001	0941	0947	2	384	2	> 250				+	+	72	Y	Y	
5	**RFE**	**15.12.2001**	**1003**	**1058**	**17**	**3264**	**2**	**> 250**		**X**	**X**	**+**	**+**	**73**	**Y**	**Y**	**O**
6	**RFE**	**16.12.2001**	**0731**	**0737**	**2**	**384**	**4**	**> 250**				**+**	**+**	**44**	**Y**	**Y**	**O**
7	**RFE**	**16.12.2001**	**0803**	**0852**	**15**	**2880**	**1**	**> 250**				**+**	**+**	**60**	**Y**	**Y**	**O**
8	**RFE**	**16.12.2001**	**0839**	**0848**	**3**	**576**	**1**	**> 250**				**+**	**+**	**80**	**Y**	**Y**	**O**
9	**RFE**	**16.12.2001**	**0852**	**0930**	**12**	**2304**	**1**	**> 250**		**X**	**X**	**+**	**+**	**61**	**Y**	**N**	**O**
24	FS	16.12.2001	0944	0950	2	384	3	> 250				+	+	67	Y	Y	
10	**RFE**	**16.12.2001**	**1016**	**1045**	**9**	**1728**	**3**	**> 250**	**N**	**X**		**+**	**+**	**79**	**Y**	**Y**	**O**
25	FS	16.12.2001	1029	1035	2	384	2	> 250				–	+	94	Y	Y	
11	**RFE**	**16.12.2001**	**1051**	**1059**	**3**	**576**	**3**	**> 250**			**X**	**+**	**+**	**89**	**Y**	**Y**	**O**
26	FS	17.12.2001	1010	1013	1	192	3	0–250				+	+	86	Y	Y	
27	FS	17.12.2001	1017	1020	1	192	3	0–250				+	+	76	Y	Y	
12	**RFE**	**18.12.2001**	**0643**	**0650**	**2**	**384**	**1**	**> 250**				–	**+**	**118**	**N**		**O**
13	**RFE**	**18.12.2001**	**0754**	**0803**	**3**	**576**	**1**	**> 250**			**X**	–	**+**	**160**	**Y**	**Poor**	**O**
14	**RFE**	**18.12.2001**	**0938**	**1007**	**9**	**1728**	**3**	**> 250**	**N**	**X**		–	**+**	**140**	**Y**	**Y**	**O**
15	**RFE**	**18.12.2001**	**0951**	**1020**	**9**	**1728**	**3**	**> 250**	**N**	**X**		–	**+**	**157**	**Y**	**Y**	**O**
16	**RFE**	**18.12.2001**	**1007**	**1030**	**7**	**1344**	**3**	**> 250**	**N**	**X**		–	**+**	**170**	**Y**	**Y**	**O**
28	FS	19.12.2001	0841	0847	2	384	3	0–250				–	–	180	N		
17	**RFE**	**20.12.2001**	**0619**	**0622**	**1**	**192**	**1**	**> 250**				–	**+**	**102**	**Y**	**Poor**	**O**
29	FS	20.12.2001	0651	0657	2	384	1	> 250				+	+	83	Y	Y	
30	FS	20.12.2001	1016	1025	3	576	3	> 250				–	+	128	Y	Y	
18	**RFE**	**20.12.2001**	**1025**	**1051**	**8**	**1536**	**3**	**> 250**	**N**	**X**		–	**+**	**150**	**Y**	**Y**	**O**
19	**RFE**	**20.12.2001**	**1041**	**1057**	**5**	**960**	**3**	**> 250**			**X**	–	**+**	**105**	**Y**	**Y**	**O**
20	**RFE**	**21.12.2001**	**0738**	**0755**	**5**	**1280**	**3**	**> 250**		**X**		–	**+**	**113**	**N**		**A**
21	**RFE**	**21.12.2001**	**0855**	**0912**	**4**	**1024**	**3**	**> 250**				–	**+**	**156**	**N**		**A**
31	FS	21.12.2001	0929	0938	2	384	3	0–250				–	+	157	N		

along with (A) or opposite to (O) the direction of the IMF B_Y controlled magnetic tension force. For a positive (negative) IMF B_Y newly opened field lines are dragged by the magnetic tension force to the west (east) in the Northern Hemisphere before they convect tailward across the polar cap driven by the solar wind flow [*Heppner and Maynard*, 1987].

4.2. Data Analysis Results

[37] Throughout the data set the ion velocity exhibited much fine structure. In total 21 RFEs were identified in 123 of the 767 scans, meaning that they occur in 16% of the scans. Flow structures that failed to satisfy one or more of these strict criteria were registered separately and occurred in 7.8% of the scans. There may be no principal difference between the two, despite the fact that flow structures do not fully develop into RFEs for still unknown reasons.

[38] The average lifetime of RFEs was ~19 min. This lifetime includes (if observed) the growth and decay of RFEs, during which the ion flow not necessarily has to be reversed but may only be a reduction of the background convection. Almost every fourth RFE was however cut short as the radar field of view was altered to observe in a different azimuth sector. This obviously influences the

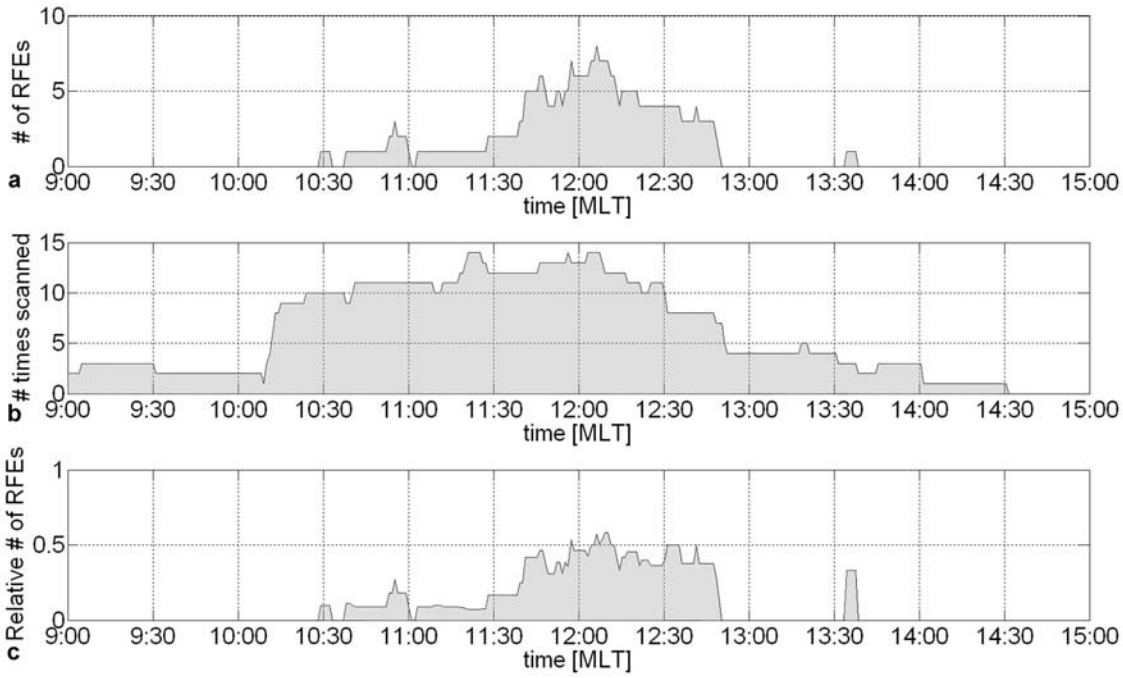

Figure 4. (a) The counted number of RFEs versus MLT corresponding to the radar fan midposition. The curve represents how many times an RFE was observed during a 1 min interval integrated over the entire data set. (b) Data coverage as a function of MLT corresponding to Figure 4a. For example if the radar scanned from 0900 until 1200 MLT, the number of times this region was scanned was augmented by one for every minute from 0900 until 1200 MLT. (c) Relative occurrence of RFEs with respect to the data coverage. This plot was inferred by dividing the RFE occurrence versus MLT (Figure 4a) by the number of times any given MLT minute had been scanned (Figure 4b).

calculated average lifetime. Four very long lived RFEs were found, each lasting for 28 min and hence ~10 min longer than the average lifetime of 19 min. They developed from a small-scale reduction of the background flow into a large RFE. One of these four RFEs is shown in Figure 1. The background flow in the ESR field of view was relatively uniform during these four RFEs. From a study like the one presented here, it is not possible to further parameterize the lifetime of RFEs. Around 30% of the RFEs exhibited latitudinal, poleward motion during their lifetime and all except one of these RFEs occurred during IMF B_Z negative. Around ~50% of the RFEs widened, but there was no correlation with IMF B_Z. However, no relationship between motion and widening has been found.

4.2.1. Quadrant Appearance of RFEs

[39] Of the time scanned in each of the four quadrants, the relative frequency of occurrence of RFEs was much higher in the first and third quadrant (Q1 and Q3) than in the second an fourth (Q2 and Q4), and RFEs occurred more than twice as often in Q3 than in Q1. In the context of the SuperDARN large-scale convection maps the RFEs were located in regions of enhanced plasma convection close to or within the cusp inflow region. Furthermore, it became clear that all events did have a nonzero IMF B_Y component with a large zonal flow component. During moderate activity the dayside auroral oval is centered on 75° MLAT, i.e., close to Longyearbyen. Owing to the dipole tilt, the auroral oval is oriented along the diagonal of Q1 and Q3 in Figure 1. Q4 will only be covered by aurora in case of an expanded polar cap. Similarly, the cusp may be situated in Q2 only when the polar cap is contracted. In cases where the zonal flow along the auroral oval dominates (large IMF B_Y) the ESR will, owing to geometry of the line-of-sight velocity measurements, be most sensitive to RFEs in Q1 and Q3 but not in Q2 and Q4 (cf. section 3.2).

[40] Examining the occurrence of flow structures, it is apparent that flow structures actually occurred most frequently in Q2. It seems as if the low appearance of RFEs in Q2 may be related to the fact that the ESR is less sensitive to Q2 for a nonzero IMF B_Y as discussed above.

4.2.2. MLT Occurrence of RFEs

[41] The ESR field of view spans over 2–4 hours in MLT depending on the azimuth range, and the RFEs often exceed the field of view. In order to derive the MLT occurrence of RFEs, the start and stop times of the RFEs inferred from Table 2 have been adjusted to account for the actual MLT of the measurements at the midposition in longitude of each ESR scan (listed in Table 1 column 10).

[42] The resulting MLT occurrence of RFEs was determined, and is shown in Figure 4. Figure 4a shows how many times an RFE was observed at a certain MLT throughout the data set, binned in minutes. The figure revealed that the maximum occurrence of RFEs was around 1200 MLT but skewed slightly over toward postnoon. The activity peaked with a total number of eight RFEs around 1215 MLT. No activity occurred before 1030 MLT and activity was low with on average one RFE occurring between 1030 and 1130 MLT, before it tripled from two

to six RFEs just after 1130 MLT. The RFE activity was high with four to eight RFEs between 1145 and 1245 MLT, before a steep decrease to zero just prior to 13 MLT. One event occurred around 1330 MLT.

[43] However, our database does not have uniform coverage between 0900 and 1500 MLT. Hence, Figure 4b indicates how many times the radar has scanned a certain MLT throughout the data set, binned in minutes. The figure reveals that the ESR scanned the region between 1015 and 1245 MLT more than five times (mostly around 10 times), whereas the regions between 0900 and 1015 MLT and 1245 and 1430 MLT were scanned less than five times. Hence a relative occurrence plot for RFEs has been generated and is shown in Figure 4c. In Figure 4b the number of RFEs at a certain MLT has been divided by the number of times the ESR has actually scanned that MLT. From Figure 4c it can be seen that the RFE activity onset occurred at 1030 MLT and was low between 1030 and ~1145 MLT. Please note that one single RFE occurred during an interval of low data coverage postnoon. Not much importance should be paid to the size of such a single-event peak. At 1145 MLT the activity increased steeply and remained high until a steep decrease at ~1245 MLT. During this time period RFEs were observed in 40% of the scans. Comparing Figures 4b and 4c, the increase of activity prenoon occurred in a region of high data coverage, but the steep decrease of event occurrence in the postnoon sector before 1300 MLT coincides with a steep decrease in data coverage. Hence the distribution on the postnoon side may be strongly affected by data coverage.

[44] Since IMF B_Y was predominantly positive in the available data set, the apparent postnoon shift of the RFE activity occurrence is consistent with RFEs being a cusp related phenomena, as the active cusp is expected to be shifted toward postnoon for positive B_Y [*Cowley et al.*, 1991].

[45] Placing the RFEs in the context of SuperDARN polar cap convection patterns showed that RFEs most often appeared in the cusp inflow region postnoon, near the equatorward border strong convection.

4.2.3. IMF Dependency and Ion Flow Direction With Respect to the Magnetic Tension Force

[46] The entire data set was biased toward IMF B_Y positive, and only 8.7% of the time, B_Y was negative. In total, 2 RFEs (9.5%) occurred during an interval of negative IMF B_Y. The IMF B_Z component was negative 57.2% of the time, and 14 RFEs (66.6%) occurred during an interval of negative B_Z. It seems thus as if the occurrence is independent of IMF B_Z. For IMF B_Y the number of scans and events involved is really too low to determine the B_Y polarity dependence. However, the occurrence of RFEs is not exclusively related to one IMF B_Y polarity. All RFEs and flow structures occurred in the clock angle range between 40° and 240°.

[47] The ion flow direction of RFEs was defined to be in the opposite direction of the background flow observed in the ESR field of view. Furthermore, 85.7% of the time (18 RFEs) the RFE flow direction was opposite to the direction of the magnetic tension force suggested by IMF conditions. This is illustrated with the RFE in Figure 1. The time shifted IMF for the actual time interval is shown in Figure 3. The RFE shown in Figure 1 takes place from 1016 to 1045 UT, thus in an interval of clearly positive IMF B_Y. Hence newly opened field lines would experience a pull dawnward. The ion flow direction of the RFE shown in Figure 1 however is clearly "blue" and hence duskward. Looking at the background flow in the ESR field of view, and comparing it to the SuperDARN plot for the actual time interval (Figure 2) shows that the background flow is uniform and directed dawnward, as expected for positive IMF B_Y. Moreover, the RFE is located in a region of enhanced dawnward plasma flow observed by SuperDARN.

[48] SuperDARN had good coverage for 17 of the 21 RFEs (81%), poor coverage for one RFE (5%), and no coverage for three RFEs (14%). The background flow seen by the ESR was confirmed by SuperDARN for 15 of the 17 RFEs (88%) with good coverage and for the one RFE with poor coverage. If the three RFEs without SuperDARN coverage are excluded, 17 of 18 RFEs (94.4%) had a flow opposite to the magnetic tension force. If only the 15 RFEs where SuperDARN had a sufficient coverage and was moreover confirming the background flow observed by the ESR are considered, 15 of 15 RFEs (100%) exhibit an ion flow opposite to the magnetic tension force.

5. Discussion: RFEs as Southwood FTE?

[49] The MLT occurrence and the location of RFEs with respect to the large-scale polar cap convection monitored by SuperDARN indicate that RFEs indeed are a regular phenomenon occurring near cusp inflow region. It is therefore reasonable to consider RFEs as a possible signature of reconnection events. The RFEs in this study were observed within the clock angle range between 40° and 240°, which is within the clock angle range for reconnection bursts at the magnetopause reported by *Neudegg et al.* [2000].

[50] However, since the ion flow direction of RFEs is per definition opposite to the large-scale convection and the IMF B_Y controlled magnetic tension force pulls on newly opened field lines, they can definitely not be interpreted in terms of the centre flux in an FTE twin-vortex flow pattern. If RFEs relate to the Southwood FTE model, they must correspond to the return flow, as suggested by *Oksavik et al.* [2004]. From the RFE definition in section 3.2, RFEs have to extend over at least 400–600 km in the ESR field of view. The longitudinal extent of almost all RFEs exceeded the ESR field of view and hence it seems as if RFEs usually exceed 600 km in length. Since the longitudinal dimension of the return flow would have to be approximately equal to the longitudinal extent of the centre flux according to the Southwood model, the spatial dimensions appear consistent with those suggested by *Lockwood et al.* [1990].

[51] The Southwood model predicts however two return flow channels; one on the equatorward edge and one on the poleward edge of the center flux. This means that the footprint of a single FTE in the ionosphere should consist of three flow channels, one in the newly open flux area with direction determined by the magnetic tension force and two flow channels of reduced or reversed return flow.

[52] Throughout the entire data set, only three occasions were identified in which two RFEs coexisted within the ESR field of view. Since these occasions were similar, only one of them, which was presented by *Oksavik et al.* [2004, 2005], is discussed in more detail and shown in Figure 5.

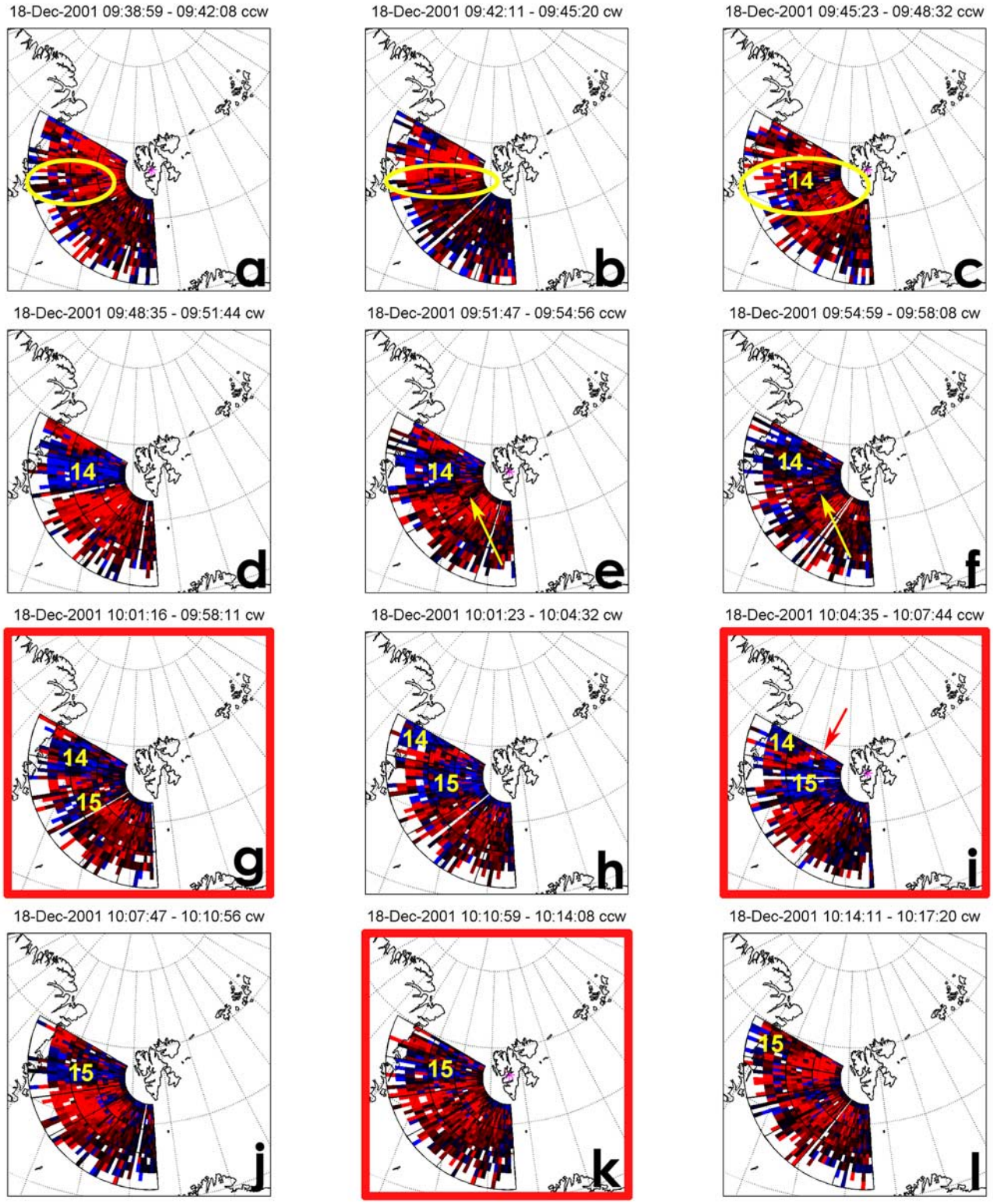

Figure 5. (a–l) A sequence of ion velocity fan plots from 18 December 2001 in geographic coordinates, covering the development of RFE 14 and RFE 15 (same format as Figure 1). The scans presented by *Oksavik et al.* [2004] are framed red. The first signs of RFE 14 are encircled by a yellow ellipse in Figures 5a–5c; the first signs of RFE 15 are indicated by a yellow arrow in Figures 5e and 5f. The red arrow in Figure 5i indicates the Southwood center flow as interpreted by *Oksavik et al.* [2004].

Oksavik et al. [2004] presented the scans which are framed, in Figures 5g, 5i, and 5k. They observed the signature of Southwood twin-vortex flow, where the narrow region of enhanced ion flow directed away from the radar indicated by the red arrow in Figure 5i, from 1004 to 1007 UT was classified as the signature of the center flux in the Southwood model, and the areas of flow directed toward the radar termed "RFE 14" and "RFE 15" as the return flow predicted by the Southwood model. The direction of the center flux as defined by *Oksavik et al.* [2004, 2005] is consistent with the background flow inferred from SuperDARN convection maps and the IMF B_Y controlled magnetic tension force on newly opened field lines for the given IMF conditions. However, as demonstrated in Figure 5, RFE 14 and RFE 15 did not develop simultaneously. The onset of RFE 14 occurred at 0938 UT, when reversed flow became visible; marked out by the yellow ellipse in Figure 5a. This flow signature grew in size and developed into a large and strong RFE at 0948 UT, Figure 5d. Some minutes later, at 0951 UT, a second region of reversed flow became visible and is indicated by the yellow arrow in Figure 5e. It rapidly developed into RFE 15. RFE 14 and RFE 15 coexisted from 0951 to 1007 UT (Figures 5e–5i). After 1007 UT, RFE 14 moved out of the field of view. Even though two RFEs coexisted inside the ESR field of view for some time, they did not develop simultaneously but with a ~13 min delay in onset.

[53] According to the Southwood FTE model, the return flow from a newly reconnected field line moving through the ionosphere is expected to occur simultaneously, and hence the two RFEs cannot be regarded as the return flow channels surrounding one single event of newly opened flux but have to be regarded as separate flow events. This is also the case for the other two occasions in which two RFEs were observed to coexist in the ESR field of view. They were both characterized by a time delay in onset of ~36 and ~17 min.

[54] If one were to attempt to fit the data to a Southwood model, there remains the question why the ESR does not observe two return flow channels with simultaneous onset as predicted by the Southwood FTE model within its field of view, and which of the two return channels would be represented by the RFE. From the ESR observations alone it cannot be determined for sure on which side of the RFE the flow enhancement associated with the motion of the newly reconnected flux tube would be located. For RFE 14, however, *Oksavik et al.* [2005] presented a comprehensive set of observations using the EISCAT Svalbard radar, the

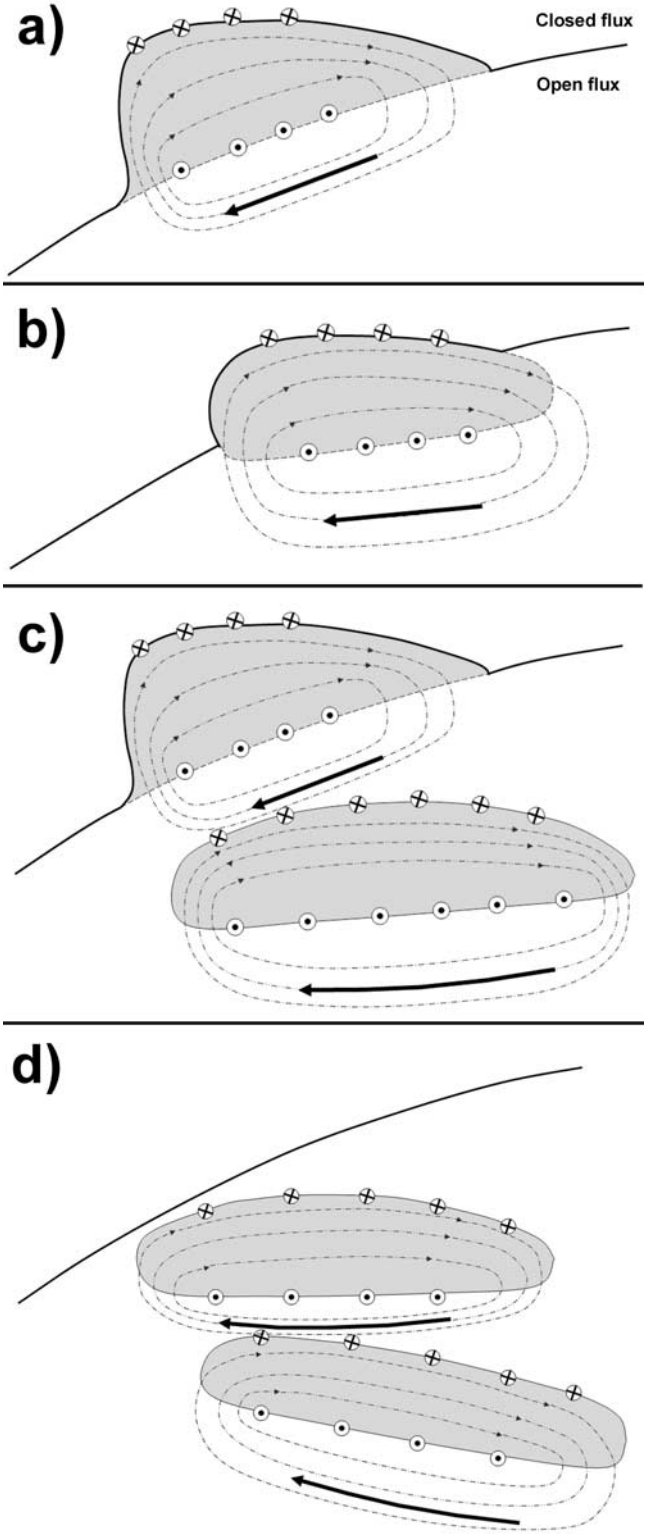

Figure 6. (a) Schematic illustration of the initial state of a suggested IMF B_Y asymmetry of the Southwood flux transfer event (FTE). The black line indicates the open-closed field line boundary, and the grey shaded region represents the region of newly opened flux due to an FTE for IMF $B_Y > 0$. Plasma streamlines are indicated by dashed-dotted arrows. Circled dots and crosses represent the location of the upward and downward field-aligned currents of the FTE current system, respectively. (b) The asymmetric Southwood model in a later state, after the magnetic tension force on the newly opened field line has pulled the field line dawnward and slightly into the polar cap. (c) A new pulse of reconnection takes place and pushes the previous reconnected flux tube further into the polar cap. (d) Both reconnected flux tubes have propagated into the polar cap and elongated due to the magnetic tension force and plasma convection.

SuperDARN HF radar network, ground-based optics, and three low-altitude polar orbiting spacecraft.

[55] At the same time as RFE 14 develops from a flow structure to an RFE in the ESR field of view over Figures 5a–5d, a region of strong, westward convection became visible at its equatorward side, consistent with the expected direction of motion of newly reconnected flux. *Oksavik et al.* [2005] found a PMAF coinciding with the equatorward edge of RFE 14, indicating an upward Birkeland current. Furthermore, a DMSP F13 satellite passage revealed the existence of a field-aligned current system with an upward Birkeland current flowing on the equatorward side of REF 14 confirming the location of the PMAF, and a downward Birkeland current on the equatorward side of the enhanced westward flow equatorward of RFE 14. These observations of FTE currents, a term inferred by *Oksavik et al.* [2005] to describe the Birkeland currents of individual flux transfer events, identify RFE 14 as the polewardmost of the two return flow channels. Hence RFE 14 and the region of enhanced westward flow equatorward of it are consistent with being the signature of the poleward clockwise cell of a Southwood FTE. RFE15 develops ~13 min after RFE14 and is as well associated with a belt of strong westward convection equatorward of it, best visible in Figures 5i and 5j. Moreover, *Oksavik et al.* [2005] found a second PMAF coinciding with the equatorward boundary of RFE 15, confirming that RFE 15 and the region of enhanced westward flow equatorward of it are consistent with being the poleward clockwise cell of a new FTE, pushing the previous FTE further into the polar cap.

[56] Since almost all RFEs observed in this study occurred during significant IMF B_Y conditions and the ESR never detected both return flow channels predicted by the Southwood model, we suggest that the Southwood model takes an asymmetric form in the case of strong IMF B_Y, in which only the poleward cell of the Southwood FTE model becomes observable. This conceptual idea of IMF B_Y asymmetry in the Southwood model is illustrated schematically in Figures 6a–6d.

[57] The grey shaded region in Figure 6a is the newly opened flux resulting from a pulse of magnetopause reconnection under large IMF B_Y positive. The open-closed field line boundary (OCB) leaps equatorward and eastward. On the flanks of the newly opened flux the FTE current system which consists of a pair of FACs is indicated by circled dots and crosses, which represent the upward and downward FACs, respectively. This current system marks off the poleward and equatorward boundary of the newly opened flux. The first force to act on the reconnected flux tube is the azimuthal magnetic stress due to IMF B_Y. The magnetic tension force initially pulls the newly reconnected flux tube westward along the adiaroic OCB. Hence the plasma pushed aside by this motion will move almost exclusively in the region of open field lines poleward of the FTE, since there cannot exist plasma flow across the OCB as indicated by the dashed-dotted plasma streamlines. A diffuse cell may, however, develop equatorward of the OCB due to induced Hall currents across the boundary. As a consequence, for significant IMF B_Y only the poleward cell of the Southwood model will develop, as observed in our data set where RFE 14 represents the poleward return flow of the first FTE. This differs from the FTE flow disturbance suggested by *Milan et al.* [2000] in their Figure 4a, which proposes a return flow channel on closed field lines, but no return flow channel on the poleward side of the upward FTE current sheet/PMAF. As the patch of newly opened flux evolves into the polar cap as indicated in Figure 6b, it elongates due to the magnetic tension and solar wind pull.

[58] A new pulse of reconnection creates a new region of open flux as indicated in Figure 6c. Its motion is initially as well determined by the magnetic tension force pull and pushes the previous FTE even further into polar cap. The first FTE is now entirely part of the older open flux in the polar cap. The grey shading is kept just to remind us about the area of flux that was added by the reconnection pulse. Owing to the current sheet on the equatorward side of the first FTE, no mixing of plasma occurs, and the two clockwise cells visible by their return flow channels RFE 14 and 15 coexist. Finally (Figure 6d), both FTEs have entirely propagated into the polar cap and form a train of cigar-shaped "recently opened flux." We think that the symmetric FTE twin cell flow pattern suggested by *Southwood* [1987] represents the situation when IMF is due south [*Cowley and Lockwood*, 1992], while the situation in Figure 6 represents the extreme of IMF B_Y dominance. The truth can be anything in between. Nevertheless, the schematic summarizes what we observe.

6. Summary and Concluding Remarks

[59] The phenomenon of transient small-scale flow channels in the cusp, observed by the ESR in a new fast scan mode, has been investigated systematically in order to reveal detailed characteristics and determine the occurrence of these features.

[60] From the discussion above it can be concluded that RFEs seem to be a regular feature of the cusp, occurring at least 16% of the time in the current data set. Since there are several constraints such as the cusp location and the limited ESR field of view, the line of sight viewing geometry with respect to the flow pattern, and a strict RFE definition, it is likely that the occurrence rate is higher. Flow structures that failed to satisfy one or more of these strict criteria were registered separately and occurred in 7.8% of the scans. Several constraints of detectability as well as the presence of less pronounced flow structures lead to the assumption that RFEs may occur even more frequently. There may be no fundamental difference between flow structures and RFEs, despite the fact that flow structures do not fully develop into an RFE for still unknown reasons.

[61] RFEs occurred near the cusp inflow region and were observed in 40% of the scans during the 60 min around 1200 MLT. They occurred in association with enhanced large-scale plasma flow observed by SuperDARN and seemed to be aligned with the auroral oval (L-shell aligned). RFEs thus seem to be a regular feature of the active cusp.

[62] The average lifetime of RFEs was 19 min. However, their lifetime can be even longer, since ~25% of the events were interrupted as the radar field of view was altered to look in a different azimuth sector. No general motion or widening could be found. Furthermore, RFEs seem to occur independently of the IMF B_Y and B_Z polarity, and for clock angles in the range of 40 to 240°. The data set is strongly biased toward IMF B_Z positive (IMF B_Y was positive for

~91% of the events). The fact that 9.5% of the RFEs occurred during IMF B_Y negative, however, indicates that the phenomenon is not exclusively related to one B_Y polarity.

[63] More than 85% of the RFEs were characterized by ion flow opposing the magnetic tension force. Since RFEs never occurred simultaneously in pairs, they cannot be interpreted as the return flow of a single Southwood twin cell FTE signature. However, an asymmetric version of the Southwood model for significant IMF B_Y conditions, where only the poleward cell located on open flux develops, has been suggested based on the observations made by *Oksavik et al.* [2005]. The asymmetry arises due to the fact that a flow vortex cannot develop across the OCB. However, owing to closure of Hall currents in the ionosphere, we believe that a diffuse cell might develop on closed flux.

[64] More observations are needed to better characterize the MLT-MLAT occurrence of RFEs and to quantify the eventual relationship to IMF orientation. The physical explanation for the RFE phenomenon will be further investigated. The discovery of RFEs by the ESR and the documentation presented here provide new and very important information about cusp dynamics that is relevant for studies of, e.g., cusp irregularities and patch formation.

[65] **Acknowledgments.** EISCAT is an international association supported by research organizations in China (CHIRP), Finland (SA), France (CNRS, until end 2006), Germany (DFG), Japan (NIPR and STEL), Norway (NFR), Sweden (VR), and the United Kingdom (PPARC). We thank the ACE Science Center and the ACE MAG and SWEPAM instrument teams for providing solar wind data from the ACE spacecraft. Financial support has been provided by the Norwegian Research Council and AFOSR task 2311AS. CUTLASS is supported the UK Particle Physics and Astronomy Research Council (PPARC), the Swedish Institute for Space Physics, and the Finnish Meteorological Institute in Helsinki. HCC wishes to acknowledge support from AFOSR under grant contract FA9550-06-1-0217, and KO is supported by NSF grant ATM-0418101.

[66] Wolfgang Baumjohann thanks Dave Neudegg and another reviewer for their assistance in evaluating this paper.

References

Carlson, H. C., K. Oksavik, J. Moen, A. P. van Eyken, and P. Guio (2002), ESR mapping of polar-cap patches in the dark cusp, *Geophys. Res. Lett.*, *29*(10), 1386, doi:10.1029/2001GL014087.

Cowley, S. W. H., and M. Lockwood (1992), Excitation and decay of solar wind-driven flows in the magnetosphere-ionosphere system, *Ann. Geophys.*, *10*, 103–115.

Cowley, S. W. H., J. P. Morelli, and M. Lockwood (1991), Dependence of convective flows and particle precipitation in the high-latitude dayside ionosphere on the X and Y components of the interplanetary magnetic field, *J. Geophys. Res.*, *96*, 5557–5564.

Denig, W. F., W. J. Burke, N. C. Maynard, F. J. Rich, B. Jacobsen, P. E. Sandholt, A. Egeland, S. Leontjev, and V. G. Vorobjev (1993), Ionospheric signatures of dayside magnetopause transients: A case study using satellite and ground measurements, *J. Geophys. Res.*, *98*, 5969–5980.

Dungey, J. W. (1961), Interplanetary magnetic field and the auroral zones, *Phys. Rev. Lett.*, *6*, 47–48.

Goertz, C. K., E. Nielsen, A. Korth, K. H. Glassmeier, C. Haldoupis, P. Hoeg, and D. Hayward (1985), Observations of a possible ground signature of flux transfer events, *J. Geophys. Res.*, *90*, 4069–4078.

Haerendel, G., G. Paschmann, N. Sckopke, H. Rosenbauer, and P. C. Hedgecock (1978), The frontside boundary layer of the magnetosphere and the problem of reconnection, *J. Geophys. Res.*, *83*, 3195–3216.

Heppner, J. P., and N. C. Maynard (1987), Empirical high-latitude electric field models, *J. Geophys. Res.*, *92*, 4467–4489.

Lockwood, M., P. E. Sandholt, S. W. H. Cowley, and T. Oguti (1989), Interplanetary magnetic field control of dayside auroral activity and the transfer of momentum across the dayside magnetopause, *Planet. Space Sci.*, *37*, 1347–1365.

Lockwood, M., S. W. H. Cowley, P. E. Sandholt, and R. P. Lepping (1990), The ionospheric signatures of flux transfer events and solar wind dynamic pressure changes, *J. Geophys. Res.*, *95*, 17,113–17,135.

Marchaudon, A., J.-C. Cerisier, R. A. Greenwald, and G. J. Sofko (2004), Electrodynamics of a flux transfer event: Experimental test of the Southwood model, *Geophys. Res. Lett.*, *31*, L09809, doi:10.1029/2004GL019922.

Maynard, N. C., E. J. Weber, D. R. Weimer, J. Moen, T. Onsager, R. A. Heelis, and A. Egeland (1997), How wide in magnetic local time in the cusp? An event study, *J. Geophys. Res.*, *102*, 4765–4776.

Milan, S. E., M. Lester, S. W. H. Cowley, and M. Brittnacher (2000), Convection and auroral response to a southward turning of the IMF: Polar UVI, CUTLASS, and IMAGE signatures of transient magnetic flux transfer at the magnetopause, *J. Geophys. Res.*, *105*, 15,741–15,755.

Moen, J., J. A. Holtet, A. Pedersen, B. Lybekk, K. Svenes, K. Oksavik, W. F. Denig, E. Lucek, and M. André (2001), Cluster boundary-layer measurements and optical observations at magnetic conjugate sites, *Ann. Geophys.*, *18*, 1655–1668.

Moen, J., M. Lockwood, K. Oksavik, H. C. Carlson, W. F. Denig, A. P. van Eyken, and I. W. McCrea (2004), The dynamics and relationships of precipitation, temperature and convection boundaries in the dayside auroral ionosphere, *Ann. Geophys.*, *22*, 1973–1987.

Neudegg, D. A., et al. (2000), A survey of magnetopause FTEs and associated flow bursts in the polar ionosphere, *Ann. Geophys.*, *18*, 416–435.

Newell, P. T., and C.-I. Meng (1992), Mapping the dayside ionosphere to the magnetosphere according to particle precipitation characteristics, *Geophys. Res. Lett.*, *19*, 609–612.

Newell, P. T., J. M. Ruohoniemi, and C.-I. Meng (2004), Maps of precipitation by source region, binned by IMF, with inertial convection streamlines, *J. Geophys. Res.*, *109*, A10206, doi:10.1029/2004JA010499.

Oksavik, K., J. Moen, and H. C. Carlson (2004), High-resolution observations of the small-scale flow pattern associated with a poleward moving auroral form in the cusp, *Geophys. Res. Lett.*, *31*, L11807, doi:10.1029/2004GL019838.

Oksavik, K., J. Moen, H. C. Carlson, R. A. Greenwald, S. E. Milan, M. Lester, W. F. Denig, and R. J. Barnes (2005), Multi-instrument mapping of the small-scale flow dynamics related to a cusp auroral transient, *Ann. Geophys.*, *23*, 2657–2670.

Pinnock, M., A. S. Rodger, J. R. Dudeney, K. B. Baker, P. T. Newell, R. A. Greenwald, and M. E. Greenspan (1993), Observations of an enhanced convection channel in the cusp ionosphere, *J. Geophys. Res.*, *98*, 3767–3776.

Rodger, A. S. (1998), Ionospheric signatures of magnetospheric processes, in *Polar Cap Boundary Phenomena,* edited by J. Moen, A. Egeland, and M. Lockwood, pp. 115–125, Kluwer Acad., Dordrecht, Netherlands.

Ruohoniemi, J. M., and K. B. Baker (1998), Large-scale imaging of high-latitude convection with Super Dual Auroral Radar Network HF radar observations, *J. Geophys. Res.*, *103*, 20,797–20,811.

Russell, C. T., and R. C. Elphic (1978), Initial ISEE magnetometer results: Magnetopause observations, *Space Sci. Rev.*, *22*, 681–715.

Russell, C. T., and R. C. Elphic (1979), ISEE observations of flux transfer events at the dayside magnetopause, *Geophys. Res. Lett.*, *6*, 33–36.

Sandholt, P. E., M. Lockwood, T. Oguti, S. W. H. Cowley, K. S. C. Freeman, B. Lybekk, A. Egeland, and D. M. Willis (1990), Midday auroral breakup events and related energy and momentum transfer from the magnetosheath, *J. Geophys. Res.*, *95*, 1039–1060.

Sandholt, P. E., C. J. Farrugia, J. Moen, Ø. Noraberg, B. Lybekk, T. Sten, and T. Hansen (1998), A classification of dayside auroral forms and activities as a function of interplanetary magnetic field orientation, *J. Geophys. Res.*, *103*, 23,325–23,345.

Shepherd, S. G., and J. M. Ruohoniemi (2000), Electrostatic potential patterns in the high-latitude ionosphere constrained by SuperDARN measurements, *J. Geophys. Res.*, *105*, 23,005–23,014.

Southwood, D. J. (1987), The ionospheric signature of flux transfer events, *J. Geophys. Res.*, *92*, 3207–3213.

van Eyken, A. P., H. Rishbeth, D. M. Willis, and S. W. H. Cowley (1984), Initial EISCAT observations of plasma convection at invariant latitudes 70°–77°, *Atmos. Terr. Phys.*, *46*, 635–641.

H. C. Carlson, J. Moen, and Y. Rinne, Department of Physics, University of Oslo, P. O. Box 1048, Blindern, N-0316 Oslo, Norway. (yvonner@fys.uio.no)

K. Oksavik, Johns Hopkins University Applied Physics Laboratory, 11100 Johns Hopkins Road, Laurel, MD 20723, USA.